







Optomechanical parametric oscillation of a quantum light-fluid latticeA. A. Reynoso ^{1,2,3} G. Usaj ^{1,2} D. L. Chafatinos ^{1,2} F. Mangussi,^{1,2} A. E. Bruchhausen ^{1,2} A. S. Kuznetsov,⁴ K. Biermann ⁴ P. V. Santos,⁴ and A. Fainstein ^{1,2,*}¹*Centro Atómico Bariloche and Instituto Balseiro,**Comisión Nacional de Energía Atómica (CNEA)–Universidad Nacional de Cuyo (UNCUYO), 8400 Bariloche, Argentina*²*Instituto de Nanociencia y Nanotecnología (INN-Bariloche), Consejo Nacional de Investigaciones Científicas y Técnicas (CONICET)–CNEA, 8400 Bariloche, Argentina*³*Departamento de Física Aplicada II, Universidad de Sevilla, E-41012 Sevilla, Spain*⁴*Paul-Drude-Institut für Festkörperelektronik, Leibniz-Institut im Forschungsverbund Berlin e.V., Hausvogteiplatz 5-7, 10117 Berlin, Germany*

(Received 14 January 2022; revised 17 April 2022; accepted 25 April 2022; published 26 May 2022; corrected 22 June 2022)

Two-photon coherent states are one of the main building pillars of nonlinear and quantum optics. They are the basis for the generation of minimum-uncertainty quantum states and entangled photon pairs, applications not obtainable from standard coherent states or one-photon lasers. Here, we describe a fully resonant optomechanical parametric amplifier involving a polariton condensate in a trap lattice quadratically coupled to mechanical modes. The quadratic coupling derives from nonresonant virtual transitions to extended discrete excited states induced by the optomechanical coupling. Nonresonant continuous-wave laser excitation leads to striking experimental consequences, including the emergence of optomechanically induced intersite parametric oscillations and intersite tunneling of polaritons at discrete intertrap detunings corresponding to sums of energies of the two involved mechanical oscillations (20- and 60-GHz confined vibrations). We show that the coherent mechanical oscillations correspond to parametric resonances with a threshold condition different from that of standard linear optomechanical self-oscillation. The associated Arnold tongues display a complex scenario of states within the instability region. The observed phenomena can have applications for the generation of entangled phonon pairs and squeezed mechanical states relevant in sensing and quantum computation and for the bidirectional frequency conversion of signals in a technologically relevant range.

DOI: [10.1103/PhysRevB.105.195310](https://doi.org/10.1103/PhysRevB.105.195310)**I. INTRODUCTION**

The concept of two-photon coherent states has been a revolutionary development in quantum optics [1]. Such states can be obtained from normal coherent states through unitary operators associated with quadratic Hamiltonians [2,3]. They correspond to the radiation states of ideal two-photon lasers operating far above threshold. In real devices, this is accomplished by using parametric processes in materials with large second-order susceptibilities [4,5]. To enhance such high-order processes, particularly in continuous-wave operation, optical parametric oscillators (OPOs) exploit a resonator so that the laser pump and either one or both parametrically generated photons (signal and idler) are confined, leading to feedback in multiwavelength cavities [6,7]. The emission of coherent entangled pairs of photons from such OPOs is at the base of different approaches for second-order correlation ($g^{(2)}$) measurements, Bell test experiments, and quantum key distribution protocols in quantum communications [8]. The mean-square quantum noise behavior of these states, which is basically the same as that of minimum-uncertainty states, leads to applications in sensing not obtainable from one-photon lasers [9–11]. Moreover, such quantum many-

photon squeezed vacuum states are involved in the most recent and promising approaches to large-scale photonic quantum computing, as an alternative to implementations using single photons [12,13].

Phonons, the quanta of mechanical vibrations, can also be used to define and manipulate coherent states. Compared with cavity photons, acoustic phonons have a longer lifetime and a much smaller wavelength (which scales with the relation of sound to light velocity), two features relevant for device integration. These properties are exploited, for example, not only in microwave-to-sound conversion and filter components based on acoustic waves, as extensively used in cell phones [14], but also with interesting prospects in quantum technologies [15]. Vacuum squeezing of the mechanical motion of solids has been reported by driving with femtosecond laser pulses materials characterized by large two-phonon Raman scattering susceptibilities [16,17]. More recently, the search for quadratic mechanical Hamiltonians (i.e., displaying a coupling quadratic in the displacement, x^2) has gained renewed interest within the framework of the rapidly developing field of cavity optomechanics [18]. A number of cavity-optomechanical systems have been explored [19], not only with the membrane-in-the-middle approach, which is probably the most paradigmatic platform [20], but also with other realizations including systems of cold atoms and levitated nanoparticles [21,22]. The x^2 coupling has been proposed

*Corresponding author: afains@cab.cnea.gov.ar

as a means for realizing quantum nondemolition measurements of phonon number [23,24], measurement of phonon shot noise [25], and the cooling and squeezing of mechanical motion [26–29].

Here, we describe a concept for the generation of two-phonon coherent states based on an optomechanical crystal of exciton-polaritons (strongly coupled light-matter particles). Exciton-polaritons behave as a quantum light fluid (LF) [30], showing Bose-Einstein condensation [31] with peculiar features stemming from their composite boson nature, effective photon-photon interactions, and the intrinsically driven-dissipative non-Hermitian character of their dynamics. Besides this, polariton condensates are interesting in the domain of cavity optomechanics due to their long coherence times and huge electrostrictive (exciton-mediated) optomechanical interactions [32–35].

We present both experimental and theoretical results for an array of micrometer-sized exciton-polariton traps on which recently polariton-driven phonon lasing has been reported [36]. We show that upon nonresonant cw excitation such a LF optomechanical lattice evolves into a stationary coexistence of condensed phases populating both the strongly localized ground state of neighbor traps and a shared delocalized excited state. The energy detuning between neighbor traps depends on the exciton reservoir because of the involved Coulomb interactions. When this detuning becomes resonant with the combined energy of pairs of phonons confined in the resonators, an optomechanical instability arising from a quadratic coupling involving the excited state sets in. The observed instability corresponds to a parametric resonance with properties fundamentally different from self-oscillation typically observed in linear-coupling resonantly driven optomechanical systems. The physics is rather that of a parametric resonator and of two-phonon coherent states conceptually equivalent to two-photon resonant OPOs well above laser threshold. Concomitant with what we define as an optomechanical parametric oscillation state, a locking of the polariton trap energies and an enhanced excited-state-mediated optomechanically induced tunneling are observed.

II. RESULTS

The light-fluid lattice. The studied system consists of cavity polaritons in micrometer-sized intracavity traps patterned by means of a shallow etch-and-overgrowth technique on a (Al, Ga)As microcavity [37]. The lateral modulation of the spacer of the microcavities creates an array of intracavity traps, each consisting of a nonetched area surrounded by etched barriers (a detailed description of the device is presented in Appendix A). These layered cavity structures also confine breathinglike vibrations polarized along the growth direction (z), with a fundamental frequency around $\nu_m^0 \sim 20$ GHz and overtones at $\nu_m^n = (1 + 2n)\nu_m^0$, $n = 0, 1, 2, \dots$ (the first one being at $\nu_m^1 = 3\nu_m^0 \sim 60$ GHz) [38]. The lateral patterning adds an additional trapping potential for acoustic phonons in a way fully equivalent to the confinement of photons. Thus, similar to polaritons, acoustic phonons can be described as confined modes of in-plane (s, p, d, \dots)-like symmetry [39]. We will concentrate here on experiments performed on an array of square traps of $1.6 \mu\text{m}$ lateral size

separated by $3.2\text{-}\mu\text{m}$ -wide etched barriers [a scheme is shown in Fig. 1(a)].

A typical spatially resolved photoluminescence (PL) image obtained below and above the polariton condensation threshold is presented in Figs. 1(c) and 1(d), respectively. The roughly $3\text{-}\mu\text{m}$ -wide Gaussian-like laser spot mainly excites a single trap. Neighboring traps are, however, also weakly excited through the tails of the laser spot as well as via lateral propagation of the excitons in the reservoir. A small unintentional misalignment of the laser spot on the addressed microstructure typically leads to one of the neighbor traps being more strongly excited than the others (the one on the left for the shown example). The fundamental and first excited states of the pumped trap, as well as weaker contributions from neighbor traps, can be identified in Figs. 1(c) and 1(d). The transition to a LF condensed state is signaled both by the narrowing of the lines and the increase of the emitted intensity from the lower confined levels [37]. Above threshold, narrow coherent emission can be identified mainly from the ground state, but also from the first excited state.

The spatial and pump power dependence of the strongly coupled polariton states in the traps can be described by a phenomenological Gross-Pitaevskii equation (GP). Since all the energy scales involved are of the same order of magnitude (exciton-photon detuning, Rabi splitting, and correlation-induced blueshift), our GP model allows for a change in the exciton-photon content as a function of the excitation power and includes the spatial modulation of the photon cavity mode energy introduced by the microstructuring of the cavity spacer (see Appendix B) [40]. From this model we can obtain the effective potential affecting the polaritons in the traps, as well as the energies and spatial distribution of the trap states. Figures 1(c) and 1(d) show, together with the experimental data, the calculated polariton effective potential, confined trap energies, and polariton modes. In the latter a significant detuning between neighbor trap states develops due to the spatially dependent blueshift induced mainly by the interaction with the reservoir. The agreement with the experiments is notably good. Importantly, intertrap overlaps between the different states, at different applied powers, can be derived from the effective potentials. For the overlap integral between ground states of neighbor traps we obtain a very small value, $\sim 10^{-4}$, highlighting a very strong localization of the ground polariton state in individual traps. This contrasts with the overlap integral between excited states, for which we obtain ~ 0.4 , evidencing that both at low and high powers the first excited state corresponds to a mode spread out in both traps.

The optomechanical sidebands. The arrays studied here display, with increasing nonresonant cw excitation power, rich optomechanical phenomena including strong phonon-assisted PL and, upon stronger excitation, very efficient mechanical coherent oscillation (phonon lasing) [36]. The latter is evidenced by the appearance of well-resolved symmetrical sidebands, separated by the energy of the fundamental mechanical breathing mode of the resonators, for both the ground- and excited-state emission [shown in Fig. 1(e)]. Quite notably, the mentioned mechanical sidebands, signaling the passage to a coherent phonon state, appear when one of the neighbor traps is red detuned with respect to the pumped trap by an integer multiple of the fundamental breathing

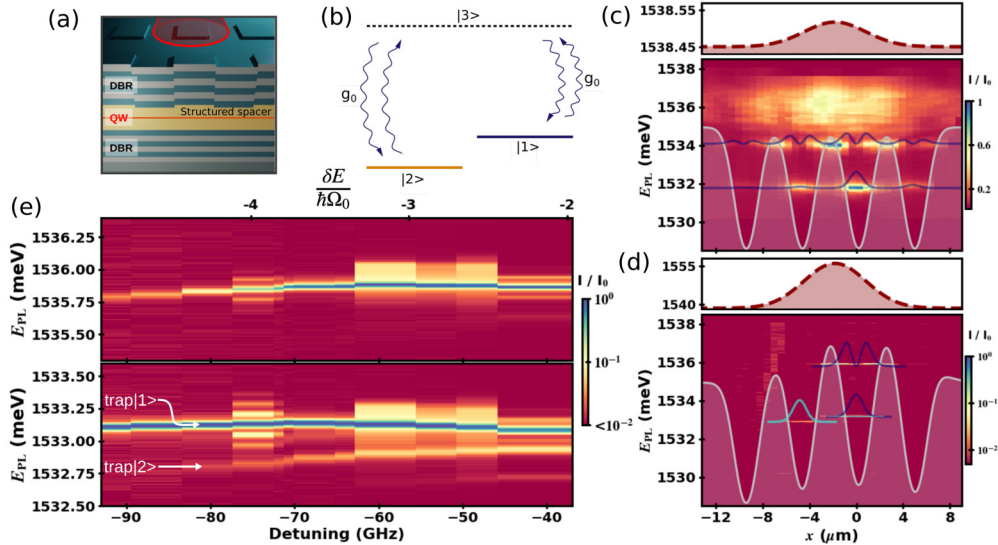


FIG. 1. Polariton effective potentials and optomechanical sidebands. (a) is a scheme of the lattice consisting of a pumped central polariton trap and neighbor traps in a square array. DBR, distributed Bragg reflector; QW, quantum well. (b) presents the involved polariton levels corresponding to the strongly confined ground states of the pumped trap ($|1\rangle$) and one of its neighbor traps ($|2\rangle$), as well as a delocalized excited state ($|3\rangle$). g_0 is the linear optomechanical interaction coupling the s -symmetric ground states with the p -symmetric excited state with the concomitant emission of a p -like confined phonon. (c) [(d)] displays the spectral and spatial image corresponding to the low-pump-power (high-pump-power) condition. The effective trap potentials (shaded light red), lateral distribution of the exciton energy (top dashed Gaussian curve), and corresponding confined polariton wave functions (thin colored curves) derived from a Gross-Pitaevskii modeling of the quantum light fluid are also shown. The detuning between the pumped and neighbor trap ground states (δE) can be tuned through the excitonic-related repulsive interaction with the reservoir by varying the nonresonant incoherent pump power as shown in (e) (note that this detuning is given in units of the phonon energy $\hbar\Omega_0$ in the top scale). The emission from ground states $|1\rangle$ and $|2\rangle$ and the excited state $|3\rangle$ can be identified. Note that clear and symmetrical spectral sidebands appear for both the ground and excited state precisely when one of the neighbor traps is red detuned with respect to the pumped trap by integer multiples 2 and 4 of the fundamental breathing mechanical cavity mode $\nu_m^0 \sim 19$ GHz.

mechanical cavity mode energy $\hbar\nu_m^0$ [36]. More precisely, they occur at $\delta E_4 = -4\hbar\nu_m^0$ (~ 75 GHz) and $\delta E_2 = -2\hbar\nu_m^0$ (~ 37 GHz)—experimental spectra for these detunings are shown in Figs. 2(a) and 2(b), respectively. These observations clearly point to a resonant two-mode optomechanical system, involving the polariton ground states of the pumped and a neighbor trap, and the mechanical breathing oscillation of the optical cavities. We note that a strong modification of both the ground- and excited-state spectra in Fig. 1(e) can also be observed for detunings $\delta E \sim 50$ – 60 GHz ($\sim 3\hbar\Omega_0$). The states in this case, however, do not display symmetrical well-resolved sidebands, but an asymmetric distortion of a different nature.

The standard approach for optomechanical linear coupling (cavity-phonon coupling proportional to x) based on a two-mode cavity system leads to the optomechanically modified phonon effective linewidth $\Gamma_{\text{eff}} = \Gamma_m(1 - C)$, where Γ_m is the original phonon linewidth and C is the so-called optomechanical cooperativity [18]. This result holds when the two polariton modes of energy $\hbar\omega_i$ are detuned by the phonon energy $\hbar\Omega_0 \equiv \hbar\nu_m^0$, that is, for $\omega_1 - \omega_2 = \Omega_0$. We use here the trap index $\{1, 2\}$, where 1 (2) refers to the pumped (neighbor) trap. To derive Γ_{eff} , a strong coherent driving tuned to the blue-shifted polariton mode 1 is also assumed while cavity losses are included through the optical linewidths $\kappa_i = \kappa$ of the polariton traps. It follows that for such two-mode resonant linear optomechanical systems, the threshold for self-oscillation is reached provided that $1 < C = 4 \frac{n_1 |g|^2}{\kappa \Gamma_m}$, where g is the optomechanical single po-

lariton coupling rate and n_1 is the occupation of the driven mode.

The optomechanical factor coupling polariton levels of the same trap can be estimated to be in the range $g/2\pi \sim 0.05$ – 5 MHz [35,38,41], depending on the degree of radiation pressure or resonant electrostrictive contribution to the coupling (see Appendix C)—hereinafter we refer to this value as g_0 to emphasize its on-site character. For the two-mode situation described by our experiments, however, the optomechanical coupling g connecting ground states of separate traps should be much smaller because of the mentioned overlap integrals being of the order of 10^{-4} . Confined LFs act as an intracavity coherent source. It turns out, however, that because of the mentioned strongly isolated character of the polariton ground states, and being that $C \propto |g|^2$, the optomechanical cooperativity based on these calculations is several orders of magnitude smaller than the one required to account for the observed threshold to mechanical self-oscillation, even considering the upper limit of resonant electrostrictive contribution. Moreover, we note that the phonon sidebands are observed when the detuning between traps is *not* $\hbar\Omega_0$, but an even multiple ($n = 2, 4$) of it.

Mechanical mode softening, intertrap frequency locking, and enhanced tunneling. We now address additional features that arise in connection with the resonant intercavity detunings δE_4 and δE_2 . Figures 2(a) and 2(b) present the emission spectra corresponding to these two resonance conditions in which symmetrical evenly spaced mechanical sidebands are

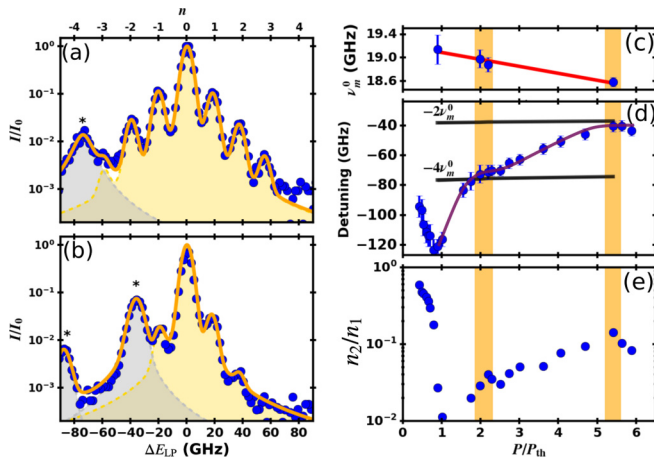


FIG. 2. Mechanical mode softening, intertrap frequency locking, and enhanced polariton transfer. Examples of PL emission precisely at the resonant detuning conditions $\delta E_4 \sim 75$ GHz and $\delta E_2 \sim 37$ GHz are shown in (a) and (b), respectively. Asterisks indicate PL from neighbor traps. The symmetric evenly spaced mechanical sidebands can be clearly observed at detunings corresponding to integer numbers $n = 2$ and $n = 4$ of the fundamental mechanical frequency $\hbar\Omega_0$. Fits to the spectra [indicated with continuous orange curves in (a) and (b)] allow for the derivation of the applied incoherent nonresonant cw pump power dependence of the involved mechanical frequencies, the trap energy detuning, and their occupation [shown in (c)–(e), respectively]. The vertical yellow bands indicate the regions where the intertrap resonances are attained, leading to the observation of the mechanical sidebands.

observed. The asterisks in these panels indicate peaks related to PL coming from neighbor traps (also highlighted with a darker shading). Phenomenological Lorentzian fits to the main lines and phonon-related sidebands in the polariton emission spectra allow for the determination of the phonon frequency, the intertrap detuning, and the relative ground-state occupation of the neighbor traps when the power of the nonresonant pump is varied. These three features are displayed in Figs. 2(c)–2(e). Vertical orange bands identify the powers at which mechanical sidebands are observed. There is a softening of the phonon frequency as the power is increased [Fig. 2(c)], amounting to about 1–2% over the whole scanned power range. Such softening resembles the so-called optical spring effect typical of back action in cavity optomechanical phenomena [18]. The intertrap detuning shown in Fig. 2(d) is in principle determined by the distinct blueshift of the pumped and the neighbor trap ground states induced by interactions between confined LFs and the excitonic reservoir. Quite notably, close to the first mechanical instability regime at $\delta E_4 \sim 75$ GHz, the rapidly evolving detuning changes its slope, partially locking around this value for a range of applied powers. After a further increase of the applied power, the reappearance of a mechanical coherent state coincides with the final locking of the detuning at $\delta E_2 \sim 37$ GHz. This behavior, indicative of a locking of the intertrap energy detuning at an energy scale defined by the optomechanics, is highlighted in Fig. 2(d) with a guide-to-the-eye continuous curve superimposed on the data.

The information concerning the intertrap polariton transfer, on the other hand, is reflected in the intensity of the lines in the

emission spectra as a function of increasing power (i.e., as a function of trap detuning), as displayed in Fig. 2(e), where the relative occupancy n_2/n_1 is shown (note the log scale). Here, n_1 and n_2 are the occupancy of polariton mode 1 and mode 2, respectively. Note that maxima of n_2/n_1 are observed when the instability to a mechanical coherent state occurs, bringing evidence of an enhanced polariton tunneling from the pumped to the neighbor trap when the peculiar resonant conditions are met. The origin of such resonant mechanical instability at detunings corresponding to multiples of the phonon frequency, the mechanical mode softening, the intertrap locking, and the optomechanically induced polariton tunneling will be addressed next.

Model Hamiltonian for a trap array with optomechanical coupling mediated by an excited state. To describe the appearance of optomechanical induced sidebands on the PL spectrum of the nonresonantly pumped trap array, we introduce here a simplified model that captures the main physical ingredients. The model takes into account the two fundamental polaritonic modes of two neighboring cavities, a single polariton excited state shared by both traps and an on-site phonon-mediated coupling between ground and excited states. The Hamiltonian then has two contributions, $H = H_0 + H_{OM}$. Here,

$$H_0 = \sum_{j=1}^3 \hbar\omega_j \hat{a}_j^\dagger \hat{a}_j + \sum_n \hbar\Omega_n \hat{b}_n^\dagger \hat{b}_n \quad (1)$$

describes the decoupled polariton and phonon modes: (i) \hat{a}_j^\dagger (\hat{a}_j) creates (annihilates) a polariton in the j mode with energy $\hbar\omega_j$, where $j = 3$ refers to the excited mode; and (ii) \hat{b}_n^\dagger (\hat{b}_n) creates (annihilates) a p phonon in the n mode with energy $\hbar\Omega_n$. The index n labels the fundamental and the overtone mechanical modes so that, for example, $\Omega_1 = 3\Omega_0 \sim 2\pi \times 60$ GHz (for simplicity, we take $\Omega_0 = 2\pi \times 20$ GHz). The linear optomechanical coupling reads

$$H_{OM} = \sum_{j=1}^2 \sum_n \hbar g_{jn} (\hat{a}_j^\dagger \hat{a}_3 + \hat{a}_3^\dagger \hat{a}_j) (\hat{b}_n^\dagger + \hat{b}_n). \quad (2)$$

Note that there is no direct coupling between \hat{a}_1 and \hat{a}_2 ; this occurs only with the excited mode. This is so because tunneling between the fundamental modes is negligible, and so is the direct optomechanical coupling constant. Because of the fully symmetric s character of the traps' ground state and the p symmetry of the polariton excited state, only acoustic phonons of p symmetry need to be considered— s modes couple to the number operator $\hat{a}_j^\dagger \hat{a}_j$, and their role will be discussed below (see also the discussion in Appendix D). In addition, we note that while the s -like mechanical vibrations turn out to be fully confined, the p phonon modes are extended and so shared between traps (as the excited polariton state).

It is straightforward to derive from the above Hamiltonian the equations of motion for \hat{a}_j and for the dimensionless phonon displacement operator, $\hat{x}_n = \hat{b}_n^\dagger + \hat{b}_n$. Here, we restrict ourselves to the semiclassical approximation, where the bosonic operators are replaced by complex functions, which implies that the solution of interest contains a large number of both polaritons and phonons and so quantum fluctuation can be ignored. The dynamics of the system is then given by the

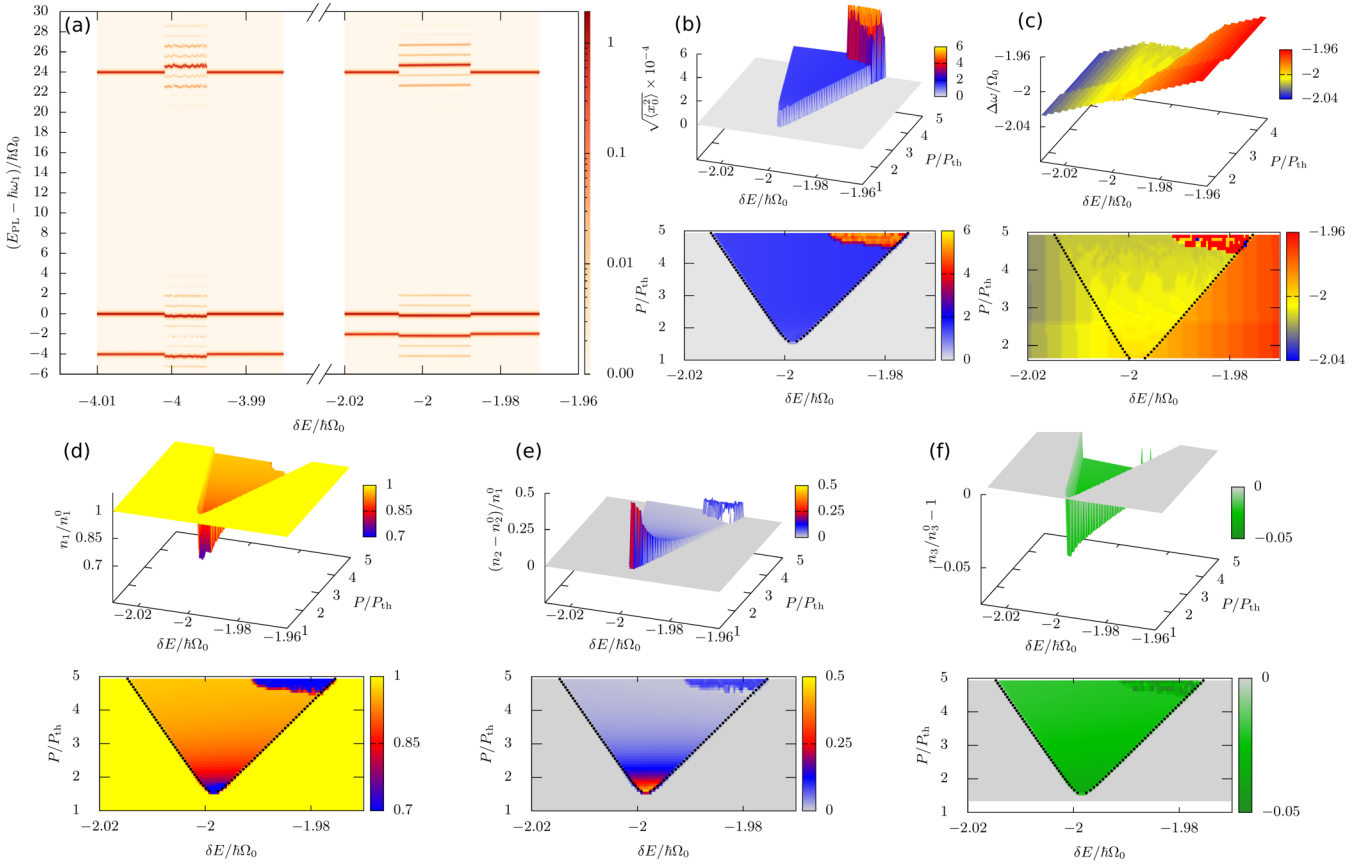


FIG. 3. Optomechanical instability and Arnold tongues of the effective parametric resonator. (a) shows the calculated PL spectra for the Hamiltonian $H_0 + H_{OM}$, as a function of the bare detuning δE between traps 1 and 2. Here we set $\omega_1 = 0$, $\omega_2 = \delta E/\hbar$, $\omega_3 = 24\Omega_0$, and the threshold power as indicated in the main text. Optomechanical instabilities are observed at $\delta E = -4\hbar\Omega_0$ and $\delta E = -2\hbar\Omega_0$, corresponding to resonances involving the fundamental and first overtone of the mechanical vibrations ($\Omega_1 \pm \Omega_0$), or two fundamental mechanical vibrations ($2\Omega_0$), respectively. The resolved additional peaks appear around both the ground and excited states and are separated by the frequency of the fundamental mode (Ω_0). As a function of trap detuning, and depending on the occupancy of the involved levels n_1 and n_2 , instability (stability) regions can be defined characterized by the presence (absence) of coherent mechanical oscillations. The instability regions correspond to so-called Arnold tongues of a parametric resonator, with characteristic stationary values of $\sqrt{\langle x_0^2 \rangle}$, which is proportional to the square root of the phonon number (b), the dressed cavity detuning $\Delta\omega$ (c), and the traps' level occupation, as displayed in (d)–(f). Note in (d) and (e) the strong optomechanically enhanced transfer of polaritons from trap 1 to trap 2 and in (c) the locking of their relative detuning within the instability region to the resonant value given by the sum of the two involved vibrations. Dotted lines in the color maps indicate the boundary of the Arnold tongue as estimated from Eq. (9).

set of coupled nonlinear equations detailed in Appendix D. In order to describe the effective non-Hermitian dynamics, we added a phenomenological term in the equations to account for the incoherent driving of the polariton modes induced by the excitons in the reservoir having decay rate γ_R [see Eq. (D2)]. Such a stimulated driving leads to an effective decay rate for the polaritons $\tilde{\kappa}_j = \kappa_j[1 - (P_j/P_{th,j})]/(1 + |a_j|^2\bar{R}/\gamma_R)$, which describes the condensation of each mode when the rate P_j (proportional to the creation rate of excitons in the reservoir and hence to the laser power) is larger than the threshold $P_{th,j} \equiv \kappa_j\gamma_R/\bar{R}$. Here, \bar{R} is the rate of stimulated scattering from the reservoir to the polariton modes. In the absence of optomechanical effects, each mode would condense ($\tilde{\kappa}_j = 0$) to an occupation $n_j^0 = (P_j/P_{th,j} - 1)n_0$ with $n_0 = \gamma_R/\bar{R}$. Additionally, we also include in the equations for x_n a dissipative term proportional to Γ_n (frequency linewidth) to account for the decay of the phonon modes. The derived nonlinear coupled equations were solved numerically

for different values of the parameters using the Runge-Kutta method choosing initial conditions with low phonon number. In this way we obtain steady-state solutions that are accessible when the system evolves from the low-phonon-occupation undriven condition. Attractors and multistabilities arising at a *higher* number of phonons [42] are not within the scope of this paper. We used the following realistic parameters: $g_{j0} = 3g_{j1} = 2 \times 10^{-4}$, $\kappa_j = 0.2$, $\Gamma = 5 \times 10^{-4}$, in units of Ω_0 , and $n_0 = 10^6$.

Figure 3 summarizes the most important results derived from this minimal model. Figure 3(a) presents the polariton spectrum above the threshold for optomechanical instability (to be discussed below) as a function of the detuning $\delta E/\hbar = \omega_2 - \omega_1$ between the pumped and neighbor traps. Quite notably, sidebands separated by the fundamental mechanical frequency Ω_0 occur at $\delta E_4 \sim -4\hbar\Omega_0$ and $\delta E_2 \sim -2\hbar\Omega_0$, signaling the emergence of mechanical oscillations coherently modulating the polariton states. The instability regions,

characterized by the presence of a coherent mechanical state, can be mapped by monitoring the polariton and the mechanical mode occupations, as shown around the δE_2 resonance in Figs. 3(b)–3(f)—similar features occur at δE_4 . These color maps present the stationary occupations as a function of both δE and the ratio P/P_{th} with $P_1 = P$, $P_2 = 0.65P$, $P_3 = 0.75P$, and $P_{\text{th},j} = P_{\text{th}}$. Figure 3(c) presents the detuning between the polariton traps dressed by the optomechanical interaction as a function of the same external parameters. Several interesting features can be highlighted from Fig. 3: (i) So-called Arnold tongues characterize the maps, separating the instability (inside) from the stability (outside) regions, the former characterized by the onset of a macroscopic occupation of the mechanical modes. (ii) Within these instability regions a transfer of polaritons from the ground state of the pumped trap to that of the neighbor trap is mechanically induced, even when the direct tunneling between these states is nearly zero. Note that these effects are particularly strong at the tip of the Arnold tongue, corresponding to the onset of polariton condensation. (iii) A small redshift of the mechanical vibrations with increasing optical driving is evidenced by the off-centered shape of the tongues (polaritonic dressing of the mechanical states). (iv) A locking of the polariton trap energies (main peak in the PL spectrum) at a fixed detuning that matches an integer multiple of the phonon frequency is observed within the instability regions (mechanically dressed polariton states). This locking can be connected with the universal phenomena of synchronization of nonlinear dynamical systems [43], also studied in the domain of quantum LF [44,45]. We note, however, that in our model it is purely of optomechanical nature. In fact, nonlinearities of thermal or electronic origin have not been included in the model.

Two-mode resonant cavity optomechanical system with effective quadratic coupling. To bring some light to the understanding of the described physics, and to extract the more relevant solutions of what emerges as a complex dynamics, we now discuss a further simplified model. As discussed above, the optomechanical features in the PL spectrum appear when the modes \hat{a}_1 and \hat{a}_2 are tuned to a particular energy difference (related to the phonon frequencies). This calls for a description where these two modes play the more important role. Since the excited mode is well separated from the fundamental modes in comparison with the phonon energy, $\Delta_j = \omega_3 - \omega_j \gg \Omega_n$, it is thus reasonable to assume that one can describe the dynamics with an effective reduced Hamiltonian. This can be done by means of a suitable canonical transformation. Let us define $H' = e^{-S} H e^S$, with S being an anti-Hermitian operator defined by the condition $H_{\text{OM}} = [S, H_0]$. It can be readily seen that, to leading order in g_{jn}/Δ_j and Ω_n/Δ_j , and retaining only those terms involving the phonon operators,

$$\begin{aligned}
 H' = & \sum_{j=1}^3 \hbar \omega_j \hat{a}_j^\dagger \hat{a}_j + \sum_n \hbar \Omega_n \hat{b}_n^\dagger \hat{b}_n \\
 & + \sum_{j=1}^2 \sum_{n,m} \frac{\hbar g_{jn} g_{jm}}{\Delta} (\hat{a}_3^\dagger \hat{a}_3 - \hat{a}_j^\dagger \hat{a}_j) (\hat{b}_n^\dagger + \hat{b}_n) (\hat{b}_m^\dagger + \hat{b}_m) \\
 & - \sum_{n,m} \frac{\hbar g_{1n} g_{2m}}{\Delta} (\hat{a}_1^\dagger \hat{a}_2 + \hat{a}_2^\dagger \hat{a}_1) (\hat{b}_n^\dagger + \hat{b}_n) (\hat{b}_m^\dagger + \hat{b}_m). \quad (3)
 \end{aligned}$$

Here, for simplicity, we took $\Delta_j \pm \Omega_n \sim \Delta_j \equiv \Delta$. The second line in H' reflects a coupling between the phonon displacement and the polariton mode occupations. This leads to a renormalization of the phonon energies induced by the polaritons in both the ground and excited states. When a mechanical coherent state sets in, it also leads to a modification of the polariton energies depending on the phonon occupation. The last line in H' , in turn, makes explicit that there is an effective *quadratic* phonon coupling between the two fundamental polariton modes of the neighboring traps, of order $G_2 = g_{1n} g_{2n} / \Delta \sim g_0^2 / \Delta$, since g_{jn} are of the order of the abovementioned on-site linear coupling constant g_0 . As we show below, this leads to a parametric instability of the phonon state, conceptually different from the self-oscillation observed in linear optomechanical systems, whenever the detuning δ equals the sum of energies of two mechanical modes of the system.

Parametric resonance. One can readily derive from H' the equations of motion in a fashion similar to that used for the full model (described in Appendix D). Here, we only write down the one corresponding to \hat{x}_n (in the same semiclassical limit as before):

$$\begin{aligned}
 \ddot{x}_n = & -\Gamma_n \dot{x}_n - \Omega_n^2 x_n - 4\Omega_n \sum_{j=1}^2 \sum_m \frac{g_{jn} g_{jm}}{\Delta} (a_3^* a_3 - a_j^* a_j) x_m \\
 & + 4\Omega_n \sum_m \frac{g_{1n} g_{2m}}{\Delta} (a_1^* a_2 + a_2^* a_1) x_m, \quad (4)
 \end{aligned}$$

which corresponds to a set of coupled harmonic oscillators with parametric driving. The latter becomes evident when noticing that the last two terms, for $m = n$, correspond to a time-dependent modulation of the phonon frequency. Moreover, the last term can become resonant at appropriate intertrap detunings. It is important to keep in mind that this modulation provided by the polariton modes is not given but rather obtained self-consistently by solving all the equations of motion simultaneously.

To better grasp the origin of the parametric instability and derive analytical expressions for the threshold condition, we look at the simpler situation where only one p phonon mode exists (sufficient to describe the resonance at δE_2). In that case, Eq. (4) reduces to

$$\ddot{x}_n + \Gamma_n \dot{x}_n + \tilde{\Omega}_n^2 x_n = 0, \quad (5)$$

where

$$\tilde{\Omega}_n^2 = \Omega_n^2 + 4\Omega_n \frac{g_0^2}{\Delta} \left(2n_3^0 - \sum_{j=1}^2 n_j^0 + 2\sqrt{n_1^0 n_2^0} \cos(\omega_1 - \omega_2)t \right). \quad (6)$$

Here, we took $g_{1n} = g_{2n} = g_0$ for simplicity and also assumed the zero-order solution (no phonon) for the polariton modes—that is, $a_j^0(t) = \sqrt{n_j^0} e^{-i\omega_j t}$. Equation (4) can be cast in the form of the damped Mathieu equation [46]

$$\ddot{q} + \Gamma \dot{q} + (\Omega^2 + \Omega_p^2 \cos \omega_p t) q = 0, \quad (7)$$

with $q(t) = x_n(t)$,

$$\Omega^2 = \Omega_n^2 + \frac{4\Omega_n g_0^2}{\Delta} \left(2n_3^0 - \sum_{j=1}^2 n_j^0 \right), \quad \Omega_p^2 = \frac{8\Omega_n g_0^2}{\Delta} \sqrt{n_1^0 n_2^0}, \quad (8)$$

and $\omega_p = \delta = \omega_1 - \omega_2$. This equation shows unstable solutions (parametric resonances) when $|\omega_p| \sim 2\Omega/l$, with l being an integer number. The case $l = 1$ is the standard (and most intense) double-frequency parametric resonance of an oscillator, while $l > 1$ describes the corresponding subharmonic driving conditions. Taking Ω_n as the fundamental confined mode at $\Omega_0/2\pi = 20$ GHz, this explains the experimental observation of mechanical sidebands at $\delta E_2 = -2\hbar\Omega_0$. The generalization of this result to a system with more than one phonon mode leads to resonances also at the sums of two of them (see Appendix D). The resonance at $\delta E_4 = -4\hbar\Omega_0$ can thus be understood as being due to a combination $\Omega_0 + \Omega_1$. Note also that the first line of Eq. (8) describes the variation of the mechanical frequency induced by the polaritons and explains the small shift of the center of the Arnold tongues shown in Fig. 3.

A standard stability analysis of the damped Mathieu equation [46] allows us to find the values of the detuning where the instability sets in. Assuming that the threshold condition is met, that $\Omega \gg \Gamma$ and $\omega_1 - \omega_2 > 0$, we get

$$\left| \delta + 2\Omega_n + \frac{4g_0^2}{\Delta} \left(2n_3^0 - \sum_{j=1}^2 n_j^0 \right) \right| \leq \frac{4g_0^2}{\Delta} \sqrt{n_1^0 n_2^0}. \quad (9)$$

This defines the limits of the Arnold tongues shown with dotted lines in Fig. 3, which coincide very well with the numerical solutions of the full nonlinear model. We stress that in this regime the phonon amplitude grows and the amplitudes of all fields have to be obtained self-consistently. Indeed, it turns out that the nonlinear back-action terms limit the amplitude of the phonon, thus avoiding the divergence of an ideal parametric oscillator. This occurs because the renormalization of the polariton energies induced by the mechanical coherent oscillation detunes the system from the exact parametric resonance. It is also worth mentioning that the same analytical condition can be derived directly from the original model described by H using a perturbative approach [47].

For optimal detuning, $|\delta| = 2\Omega \sim 2\Omega_n$, the threshold condition becomes

$$\frac{4g_0^2}{\Delta\Gamma} \sqrt{n_1^0 n_2^0} > 1. \quad (10)$$

Note that this expression retains some similarities with the threshold condition for self-oscillation in a two-mode linear optomechanical system, $C = 4 \frac{n_1 |g|^2}{\kappa \Gamma_p} > 1$. Firstly, it now depends on both occupations, that of the pumped and the neighbor trap. This is because what plays the role of the parametric driving in Eq. (4) is the frequency beating induced by polaritons shuttling between states 1 and 2. Secondly, it does not depend on the cavity photon (or polariton) decay rate κ . This stems from the fact that, in the studied driven-dissipative LF, the effective $\tilde{\kappa}$ becomes zero when stimulated condensation sets in. Thirdly, the second-order character of

the optomechanical coupling, which is mediated through virtual transitions to a delocalized excited polariton state, leads to an effective quadratic coupling of magnitude $G_2 = g_0^2/\Delta$. Consequently, the threshold for a parametric resonance instability is changed with respect to the linear expression by a factor of order Δ/κ . If we take for κ the inverse of the cavity photon lifetime (~ 10 ps), this number is rather small, of the order of ~ 6 . The implication is that the described mechanical instability threshold power is similar to that for an equivalent linear system, despite the fact that the direct linear coupling between isolated traps is hugely decreased due to the very small overlap integrals (the threshold power for self-oscillations in the linear optomechanical regime in our device is estimated to be several orders of magnitude larger due to this effect).

As mentioned before, we have neglected the s -phonon modes in our analysis. This is essentially correct for the sake of understanding the origin of the mechanical instability as it turns out that only the p phonon modes are responsible for the emergence of a coherent mechanical state. Nevertheless, it is important to point out that we have observed that, once the p modes become unstable, they trigger the oscillation of the s modes through the modulation of the population of the polaritonic modes at the proper frequency. When this occurs, all phonon modes can become macroscopically populated and lead to enhanced sidebands.

III. DISCUSSION AND OUTLOOK

The phenomena we have reported and termed an optomechanical parametric oscillation are different from other realizations of quadratic Hamiltonians in cavity optomechanics in several relevant aspects, as follows. (i) The term ‘‘optomechanical parametric oscillation’’ applies to optomechanical crystals that are driven, or populated, by an exciton-polariton light fluid. (ii) Concomitant with that, no resonant driving is performed: The self-oscillations arise from the intrinsic dynamics of a nonresonantly excited driven-dissipative system. (iii) The optomechanical coupling is essentially purely quadratic, with linear terms negligible for all practical purposes. (iv) It is a fully resonant two-mode light-fluid system, in which these two involved modes self-tune to the parametric resonance at double frequencies. (v) Because of the superhigh mechanical frequencies involved (20 GHz ~ 1 K, and 60 GHz ~ 3 K), the mechanical system is very close to the quantum ground state at the working standard cryogenic temperatures (~ 4 K). These peculiarities lead to some consequences that we discuss next.

Self-oscillation vs parametric resonance. A parametric resonance as described here is similar to but conceptually different from the phenomena of self-oscillation [48] present in cavity systems with linear optomechanical coupling [18]. The phenomena of self-oscillation are properties of dynamical systems characterized by a driving force that is controlled by the oscillation, acting in phase with the velocity. These phenomena can be linked also to retarded restoring forces. No explicit time dependence of the force is, however, required. In cavity optomechanical systems it leads to an additional contribution determined by the optical force to the term in the oscillator equation that is proportional to \dot{q} . Above a certain

threshold this causes a negative damping, leading to an amplitude of the oscillation that grows exponentially with time, being ultimately limited by other nonlinear effects. Parametric resonance resembles self-oscillation in that the growth of the amplitude is also exponential in time but, in this case, the equation of motion has an explicit time dependence [48]. In fact, it requires a perturbation affecting the oscillator frequency with a harmonic time dependence tuned to $|\omega_p| \sim 2\Omega/l$. In our case, this harmonic driving is intrinsically generated by the beating of a light fluid between two detuned modes belonging to neighboring traps. In this way an optomechanical parametric oscillator (OMPO) is realized, which mimics quite precisely its equivalent in optics, the optical parametric oscillator (OPO).

Limit cycles and chaos. The experimental observation of symmetrical mechanical sidebands is a manifestation of the emergence of a periodic limit cycle with the parametric oscillation characteristics just discussed. The numerical modeling of the system also evidences a more complex dynamics when the multivariable parameter space is investigated in a broader range of attainable conditions. Different phases emerge within the optomechanical instability (Arnold tongues). Notably, besides the periodic limit cycles stable within part of the parameter space, we have observed at larger excitation powers and within the Arnold tongues that there are regions characterized by chaotic-like regimes. Such chaotic phases have indeed been identified in other optomechanical systems [49–51], including resonantly driven systems with quadratic coupling [52]. The numerical simulations show that while the polariton decay rate κ does not affect the threshold for parametric oscillation (as discussed above), it does determine the peculiar geography of the different phases within the Arnold tongues.

Optomechanically induced tunneling. The reported optomechanically induced tunneling mechanism, mediated by a nonresonant excited extended state, is different from other relevant tunneling processes identified in trapped interacting bosonic condensates. The latter typically require a direct coupling between the involved initial and final states [53–58]. Based on the described optomechanically induced tunneling, phonons could be used for the control of operations in quantum simulators based on light fluids [59–62]. The optomechanical coupling, largely unexplored in the domain of exciton-polariton light fluids, can be tailored to display a rich variety of physical phenomena that could be relevant for quantum technologies.

Squeezing and two-phonon coherent states. The physics we described here is conceptually quite similar to optical parametric oscillation in photonics by which pairs of photons are generated at frequency Ω_0 through nonlinear processes induced by driving at $2\Omega_0$ in appropriate crystals lacking inversion symmetry. Indeed, the Hamiltonian for such systems takes the form $H_{\text{OPO}} = \lambda(\hat{b}^2\hat{a}^\dagger + \hat{b}^{\dagger 2}\hat{a})$, with bosonic operators \hat{a} (\hat{b}) standing for photons of frequency $2\Omega_0$ (Ω_0). The photonic driving field a is typically assumed to be large and thus taken as a complex number $a \rightarrow i\frac{r}{2}e^{-i2\Omega_0 t}$. With this, the time evolution operator of a driven OPO system, in the appropriate reference frame, essentially becomes the squeezing unitary operator $S(z) = \exp[\frac{z}{2}(\hat{b}^2 - \hat{b}^{\dagger 2})]$, where $z = \lambda r/\hbar$ here is taken as a real number. A similar proce-

cedure can be followed for our polariton system with effective quadratic optomechanical interactions when operating at the resonance $\delta E_2 \sim -2\hbar\Omega_0$, corresponding to the coupling with pairs of identical $\hbar\Omega_0$ phonons. To make a full parallel with the OPO Hamiltonian, one simply has to identify the parameters $\frac{r}{2} = \sqrt{n_1^0 n_2^0}$ and $\lambda = \frac{\hbar g^2}{\Delta}$ in Eq. (3). Under these assumptions, the mechanical wave function resulting from this polariton driving on the phonon vacuum $|0\rangle$ (the 20-GHz mode is very close to its quantum ground state at our working temperature of 4 K, with an initial thermal occupation around 4) can be expressed as a squeezed vacuum, $S(z)|0\rangle$, a two-phonon coherent state resulting from a coherent superposition of even-number states. In this sense, our system behaves as a fully resonant optomechanical parametric oscillator. In the actual device the coherent phonon population is limited both by nonlinearities of the full Hamiltonian describing the system and by the residual dephasing of the polariton condensates. The coherence time of the polariton condensates has been experimentally determined to be around 600 ps. Preliminary numerical simulations including this decoherence show that it does not modify substantially the dynamics of the system, which thus seems to be mostly limited by the intrinsic nonlinearities of the light-fluid optomechanics. We thus envision that properly designed systems might take advantage of this effective quadratic optomechanical coupling to produce entangled phonon pairs and well-defined squeezed phonon states on demand.

ACKNOWLEDGMENTS

We acknowledge partial financial support from the ANPCyT-FONCyT (Argentina) under Grants No. PICT-2015-1063, No. PICT-2018-03255, No. PICT-2016-0791, and No. PICT 2018-1509, CONICET Grant No. PIP 11220150100506, SeCyT-UNCuyo Grant No. 06/C603, the German Research Foundation (DFG) under Grant No. 359162958, and the joint Bilateral Cooperation Program between the German Research Foundation (DFG) and the Argentinian Ministry of Science and Technology (MINCyT) and CONICET. A.F. thanks the Alexander von Humboldt Foundation and the Paul-Drude-Institut for the support and hospitality while this work was completed. A.A.R. acknowledges support by PAIDI 2020 Project No. P20-00548 with FEDER funds.

APPENDIX A: DEVICE FABRICATION

The studied device consists of a microstructured polaritonic microcavity with arrays of micrometer-sized intracavity traps able to confine polaritons in three dimensions. The microcavity is created by patterning (Al,Ga)As in between growth steps by molecular beam epitaxy (MBE). The fabrication process is as follows: First a 4.43- μm -thick lower distributed Bragg reflector (DBR) consisting of thirty-six $\lambda/4$ (λ is the optical wavelength) pairs of $\text{Al}_{0.15}\text{Ga}_{0.85}\text{As}/\text{Al}_x\text{Ga}_{1-x}\text{As}$ was grown on 350- μm GaAs substrate. The Al composition x of the lower DBR is continuously reduced from 0.80 in the first stack to 0.45 in the last stack. Then, the first 120 nm of the $\text{Al}_{0.30}\text{Ga}_{0.70}\text{As}$ microcavity spacer were deposited including six 15-nm-thick GaAs quantum wells (QWs) placed at the antinode positions of the

microcavity optical mode. The structure was subsequently capped by a 170-nm-wide $\text{Al}_{0.15}\text{Ga}_{0.85}\text{As}$ layer spacer. This last layer protects the QWs for the next step, when the unfinished sample is removed from the MBE chamber and patterned by means of photolithography and wet chemical etching. Here, mesas with a nominal height of 12 nm of different shapes in the exposed spacer layer were created inducing a lateral modulation of the cavity thickness and, therefore, of the cavity energy in the final structure. Following this, the sample was reinserted into the MBE system, cleaned by exposure to atomic hydrogen, and overgrown with a $\lambda/4$ $\text{Al}_{0.15}\text{Ga}_{0.85}\text{As}$ layer. Finally, the upper DBR was grown by twenty $\lambda/4$ pairs of $\text{Al}_{0.15}\text{Ga}_{0.85}\text{As}/\text{Al}_{0.75}\text{Ga}_{0.25}\text{As}$.

The etched regions result in a blueshift of the optical cavity mode in the etched areas by 9 meV (4.5 nm) with respect to the nonetched regions. The upper surface of the etched layer spacer corresponds to a node of the optical cavity mode of the whole structure. In this way, the potential impact of roughness or impurities introduced by the *ex situ* patterning on optical properties of the structure was minimized. Furthermore, the shallow patterned layer is located more than 140 nm above the QWs, so that they remain unaffected by the processing.

The sample was designed to be in the strong-coupling regime at low temperature (~ 5 K) both in the etched and nonetched regions, leading to microcavity polaritons in these two regions with different energies and photon-exciton contents. The lateral modulation was used to create three-dimensional (square or dot potential) confinement in nonetched areas surrounded by etched barriers. A detailed characterization of the reflection and photoluminescence and the characterization of the potential profile of the polaritonic traps in this sample are presented in Ref. [37].

APPENDIX B: POLARITON MODES AND THE GROSS-PITAEVSKII EQUATION

The effective confinement potential for the polaritons and the corresponding modes shown in Figs. 1(c) and 1(d) were obtained using an effective Gross-Pitaevskii equation that takes into account both the blueshift induced by the repulsive interactions with the exciton reservoir and the saturation of the Rabi splitting [40]. Namely,

$$i\hbar \frac{\partial \psi}{\partial t} = \left[-\frac{\hbar^2}{2m_{\text{LP}}} \nabla^2 + V_{\text{LP}}(\mathbf{r}) + i \left(\frac{R P(\mathbf{r})}{\gamma_R + R|\psi|^2} - \kappa \right) \right] \psi, \quad (\text{B1})$$

where $\psi(\mathbf{r}, t)$ is the complex field describing the lower polaritons (LPs) and we have used the adiabatic approximation for the exciton reservoir [30]. Equation (B1) is a very good approximation when describing the confined polaritonic levels s and p . In addition, in our particular case, and for the purposes of describing only the energy of the polaritonic modes (not their occupation) and the effective potential, Eq. (B1) can be further simplified by ignoring the last term [40]. The effective potential is defined as

$$V_{\text{LP}}(\mathbf{r}, n_R) = \frac{1}{2}[E_C + E_X - \sqrt{\Omega^2 + \Delta^2}], \quad (\text{B2})$$

with $E_C(\mathbf{r}) = \Delta_0 + V_C(\mathbf{r})$ being the photonic potential of the trap, Δ_0 being the bare detuning, $E_X(\mathbf{r}, n_R) = g_X n_R(\mathbf{r})$ be-

ing the exciton energy ($g_X \approx 6 \mu\text{eV} \mu\text{m}^2$), and $\Delta(\mathbf{r}, n_R) = E_C(\mathbf{r}) - E_X(\mathbf{r}, n_R)$ being the effective detuning. Here, we have ignored the contribution to E_X from the repulsive interaction among the lower polaritons. This is fine in this case as the parameters are such that they have a large photonic component.

The saturation of the Rabi splitting with increasing population of the reservoir is described as

$$\Omega(\mathbf{r}, n_R) = \frac{\Omega_0}{\sqrt{1 + \frac{n_R(\mathbf{r})}{n_{\text{Sat}}}}}, \quad (\text{B3})$$

where Ω_0 is the Rabi splitting at zero carrier density and $n_{\text{Sat}} \approx 3 \times 10^3 \mu\text{m}^{-2}$. The LP effective mass is approximated as

$$\frac{1}{m_{\text{LP}}} = \frac{|X(\mathbf{r}_0, n_R)|^2}{m_X} + \frac{|C(\mathbf{r}_0, n_R)|^2}{m_C}, \quad (\text{B4})$$

where \mathbf{r}_0 corresponds to the center of the pumped trap and the spatially dependent Hopfield coefficients are

$$|X(\mathbf{r}, n_R)|^2 = \frac{1}{2} \left(1 + \frac{\Delta(\mathbf{r}, n_R)}{\sqrt{\Omega(\mathbf{r}, n_R)^2 + \Delta(\mathbf{r}, n_R)^2}} \right),$$

$$|C(\mathbf{r}, n_R)|^2 = 1 - |X(\mathbf{r}, n_R)|^2. \quad (\text{B5})$$

Note that we have explicitly taken into account the dependence of the parameters on the density of the carrier in the reservoir. The density of excitons in the reservoir as a function of the external pump power is estimated as

$$n_R(\mathbf{r}) = \frac{P(\mathbf{r})\tau_R\alpha}{\hbar\omega_L 2N_{\text{QW}}}, \quad (\text{B6})$$

where $P(\mathbf{r})$ is the pump power per unit area, τ_R is the effective lifetime of the exciton in the reservoir, α is the total effective absorption coefficient of the QWs, $\hbar\omega_L$ is the energy of the nonresonant pumping laser, N_{QW} is the number of quantum wells, and the factor 2 accounts for the dominant role of the triplet interactions. We assume a Gaussian shape for the pump given by

$$P(\mathbf{r}) = \frac{P_0}{2\pi\sigma_p^2} \exp \left[-\frac{(\mathbf{r} - \mathbf{r}_p)^2}{2\sigma_p^2} \right]. \quad (\text{B7})$$

In the simulations we use an effective value for the standard deviation $\sigma_p \approx 3 \mu\text{m}$ and change the position of the spot (\mathbf{r}_p) to reproduce the particular experimental situation. The values for Ω_0 , Δ_0 , and the cavity parameters m_C and $V_C(\mathbf{r})$ were obtained by fitting. The photonic cavity potential $V_C(\mathbf{r})$ was simulated following Refs. [37,40]. The optimal results were obtained using $\Omega_0 = 6.0$ meV and using $E_C = \Delta_0 = -10.5$ meV and $E_C = \Delta_0 + U = 5.5$ meV for the nonetched and etched regions, respectively. Here, $U = 16$ meV is the potential barrier for photons, generated by the difference in the thickness of the cavity spacer between the two regions.

APPENDIX C: OPTOMECHANICAL COUPLING CONSTANT

To estimate the linear on-site optomechanical coupling factor g_0 , corresponding to processes that couple polariton levels within the same trap, we begin by considering the

effective exciton-mediated optomechanical coupling reported in Ref. [35] for similar individual polariton traps to those investigated in this paper. This coupling results mainly from a deformation-potential interaction modulated by intense electrically generated surface acoustic waves (SAWs). A value of $g_{\text{om}}^{\text{eff}}/2\pi \sim 50$ THz/nm was obtained, which accounts for the change in polariton energy per unit of acoustic displacement [35]. This latter parameter is related to the actual on-site optomechanical coupling constant by $g_0^{\text{eff}} = g_{\text{om}}^{\text{eff}} x_{\text{zpf}}$ [18], where x_{zpf} corresponds to the displacement induced by the zero-point fluctuations. For a similar structure of $\sim 2 \mu\text{m}$ lateral size, this value has been estimated to be roughly $x_{\text{zpf}} \sim 0.5$ fm [41]. Consequently, $g_0^{\text{eff}}/2\pi \sim 50$ MHz for this system, which represents a very large value compared with other reported optomechanical systems that only account for an optical radiation back-action mechanism based on radiation pressure interaction [18]. The Hopfield coefficient for this cavity polariton trap system was of the order of $|X|^2 \sim 0.7$, and the reported structure had only one embedded QW [35].

The structure investigated in this paper has six cavity-embedded QWs instead of one, proportionally increasing the corresponding interaction of the involved fields. For the high excitation powers used for exciting the traps analyzed here, the excitonic Hopfield coefficient is estimated to be around $|X|^2 \sim 0.05$ [40]; that is, the involved polariton states have a large photonic component. Considering these two differences, the g_0 would be roughly a factor of 6 times larger and a factor 0.05/0.7 smaller with respect to the above-obtained g_0^{eff} . Therefore the on-site optomechanical coupling factor for the present work, resulting from a deformation-potential interaction, can be estimated to be $g_0/2\pi \sim 20$ MHz.

APPENDIX D: SIMPLIFIED POLARITON-PHONON MODEL

We present here the effective model used to describe the polaritons' optomechanical coupling, but now explicitly including the s phonon modes that were ignored in the main text for the sake of simplicity. The full Hamiltonian then reads

$$\begin{aligned}
 H = & \sum_{j=1}^3 \hbar\omega_j \hat{a}_j^\dagger \hat{a}_j + \sum_n \hbar\Omega_n \left(\sum_{j=1}^2 \hat{d}_{jn}^\dagger \hat{d}_{jn} + \hat{b}_n^\dagger \hat{b}_n \right) \\
 & + \sum_{j=1}^2 \sum_n \hbar g_{jn} (\hat{a}_j^\dagger \hat{a}_3 + \hat{a}_3^\dagger \hat{a}_j) (\hat{b}_n^\dagger + \hat{b}_n) \\
 & + \sum_n \sum_{j=1}^2 (\hbar \bar{g}_n \hat{a}_j^\dagger \hat{a}_j + \hbar \bar{g}_{jn} \hat{a}_3^\dagger \hat{a}_3) (\hat{d}_{jn}^\dagger + \hat{d}_{jn}),
 \end{aligned} \tag{D1}$$

where (i) \hat{a}_j^\dagger (\hat{a}_j) creates (annihilates) a polariton in the j mode with energy $\hbar\omega_j$, where $j = 3$ refers to the excited mode; and (ii) \hat{d}_{jn}^\dagger and \hat{b}_n^\dagger (\hat{d}_{jn} and \hat{b}_n) create (annihilate) a phonon in the n mode with s -like and p -like symmetry, respectively, and energy $\hbar\Omega_n$ —here we ignored the very small energy difference between the s and p modes. The index n labels the fundamental and the overtone mechanical modes so that, for example, $\Omega_1 = 3\Omega_0 = 60$ GHz. We assume the

s phonon modes to be localized on each cavity (hence the additional index j) and the p modes to be extended and so shared between cavities. Note that H_{OM} does not include a direct coupling between \hat{a}_1 and \hat{a}_2 ; this occurs only with the excited mode.

From the above Hamiltonian it is straightforward to derive the equations of motion for \hat{a}_j and for the dimensionless phonon position operators, $\hat{x}_n = \hat{b}_n^\dagger + \hat{b}_n$ and $\hat{y}_{jn} = \hat{d}_{jn}^\dagger + \hat{d}_{jn}$. In the semiclassical approximation where the bosonic operators are replaced by complex functions we obtain the following set of equations:

$$\begin{aligned}
 i\dot{a}_j &= \left(\omega_j + \sum_n \bar{g}_n y_{jn} \right) a_j + \sum_n g_{jn} x_n a_3 + F_j(a_j), \quad j \neq 3, \\
 i\dot{a}_3 &= \left(\omega_3 + \sum_{j=1}^2 \sum_n \bar{g}_{jn} y_{jn} \right) a_3 + \sum_{j=1}^2 \sum_n g_{jn} x_n a_j + F_3(a_3), \\
 \ddot{x}_n &= -\Omega_n^2 x_n - \Gamma_n \dot{x}_n - 2\Omega_n \sum_{j=1}^2 g_{jn} (a_j a_3^* + a_3 a_j^*), \\
 \ddot{y}_{jn} &= -\Omega_n^2 y_{jn} - \bar{\Gamma}_n \dot{y}_{jn} - 2\Omega_n (\bar{g}_n |a_j|^2 + \bar{g}_{jn} |a_3|^2).
 \end{aligned} \tag{D2}$$

Here, we added a phenomenological term $F_j(a_j)$ to account for the incoherent driving of the polariton modes induced by the exciton reservoir. Based on the GP, and for the purpose of introducing a stationary population of the polaritonic modes, we use the following simplified expression for it: $F_j(a_j) = i(\bar{R}P_j/(\gamma_R + \bar{R}|a_j|^2) - \kappa)a_j/2$, which immediately leads to the effective decay rate $\tilde{\kappa}_j$ introduced in the main text. This allows us to describe the condensation of each mode, when the incident power from the reservoir to mode j , P_j , is larger than the threshold power $P_{\text{th}} = \kappa\gamma_R/\bar{R}$. In the absence of the optomechanical effects, each mode would condense to an occupation $n_j^0 = (P_j/P_{\text{th}} - 1)n_0$ with $n_0 = \gamma_R/\bar{R}$. Additionally, we also included a dissipative term proportional to Γ_n and $\bar{\Gamma}_n$ (frequency linewidth) in the equations for x_n and y_{jn} , respectively, to account for the decay of the phonon modes.

The full model can be solved numerically. As mentioned in the main text, while the instability is caused by the p phonon that couples a_1 and a_2 through the excited states, once this occurs the s phonons are also excited. This leads to a renormalization of the Arnold tongues and a rich interplay between phonons, whose analysis is beyond the scope of the present work.

The description presented above, though conceptually simple and relatively easy to solve numerically, is still too complex to easily grasp the more relevant solutions. Since the excited polariton mode is well separated from the fundamental modes in comparison with the phonon energy, $\Delta_j = \omega_3 - \omega_j \gg \Omega_n$, one can describe the dynamics with an effective reduced Hamiltonian. This can be done by means of a suitable canonical transformation. Defining $H' = e^{-S} H e^S$ with S given by

$$\begin{aligned}
 S = & \sum_{j=1}^2 \sum_n \hat{a}_j^\dagger \hat{a}_3 \left(\frac{g_{jn}}{\omega_3 - \omega_j + \Omega_n} \hat{b}_n + \frac{g_{jn}}{\omega_3 - \omega_j - \Omega_n} \hat{b}_n^\dagger \right) \\
 & - \text{H.c.},
 \end{aligned} \tag{D3}$$

one gets, to leading order in g_{jn}/Δ_j and Ω_n/Δ_j and retaining only those terms involving the phonon operator,

$$\begin{aligned}
H' = & \sum_{j=1}^3 \hbar\omega_j \hat{a}_j^\dagger \hat{a}_j + \sum_n \hbar\Omega_n \left(\sum_{j=1}^2 \hat{d}_{jn}^\dagger \hat{d}_{jn} + \hat{b}_n^\dagger \hat{b}_n \right) \\
& + \sum_{j=1}^2 \sum_n (\hbar\bar{g}_n \hat{a}_j^\dagger \hat{a}_j + \hbar\bar{g}_{jn} \hat{a}_3^\dagger \hat{a}_3) (\hat{d}_{jn}^\dagger + \hat{d}_{jn}) \\
& + \sum_{j=1}^2 \sum_{n,m} \frac{\hbar g_{jn} g_{jm}}{\Delta} (\hat{a}_3^\dagger \hat{a}_3 - \hat{a}_j^\dagger \hat{a}_j) (\hat{b}_n^\dagger + \hat{b}_n) (\hat{b}_m^\dagger + \hat{b}_m) \\
& - \sum_{n,m} \frac{\hbar g_{1n} g_{2m}}{\Delta} (\hat{a}_1^\dagger \hat{a}_2 + \hat{a}_2^\dagger \hat{a}_1) (\hat{b}_n^\dagger + \hat{b}_n) (\hat{b}_m^\dagger + \hat{b}_m), \quad (D4)
\end{aligned}$$

where we used that $\Delta_j \pm \Omega_n \sim \Delta_j \equiv \Delta$. Equation (4) in the main text is derived from H' , which can be cast in the form of a Mathieu equation [cf. Eq. (7)]. This equation shows an unstable solution when $|\omega_p| \sim 2\Omega$. The stability analysis is rather standard (see, for instance, Refs. [46,47]): The condition for finding an unstable solution is given by

$$\Omega_p^2 > \sqrt{\Gamma^2 \omega_p^2 + 4 \left(\Omega^2 - \frac{\omega_p^2}{4} \right)^2}, \quad (D5)$$

from which Eqs. (9) and (10) can be obtained.

So far we considered a single Ω_0 phonon mode, which is enough to account for the resonance observed at δE_2 —for that resonance, adding the $\Omega_1 (=3\Omega_0)$ phonon leads to a complex interplay when the g_n couplings are similar. In contrast, to

describe the effects observed at δE_4 , one must consider the Ω_1 phonon. That is, one has to fully consider the two coupled oscillators that are associated with two p phonons as described in Eq. (4). As before, taking the zero-order solution for the polariton modes, one can map the equations to the ones of two damped oscillators driven by a crossed parametric excitation of frequency ω_p ,

$$\begin{aligned}
\ddot{q}_1 + \Gamma_1 \dot{q}_1 + \Omega^2 q_1 + \Omega_p^2 \cos(\omega_p t) q_3 &= 0, \\
\ddot{q}_3 + \Gamma_3 \dot{q}_3 + 9\Omega^2 q_3 + 3\Omega_p^2 \cos(\omega_p t) q_1 &= 0, \quad (D6)
\end{aligned}$$

where the coordinates q_1 and q_3 describe the oscillator having natural frequency Ω and 3Ω , respectively, $\omega_p = \omega_1 - \omega_2$, and the amplitude of the drive is given by $\Omega_p^2 = 8\Omega \frac{g_{1n} g_{2m}}{\Delta} \sqrt{n_1^0 n_2^0}$, with n and m labeling the p phonon modes with frequency 20 and 60 GHz, respectively. The frequency Ω can be assumed shifted as in the δE_2 case. By applying the two-variable expansion method [46] for $\omega_p = 4\Omega$, i.e., the frequency sum of the two coupled oscillators, we obtain the following condition for phonon instability at optimal detuning:

$$4 \frac{g_{1n} g_{2m}}{\Delta \sqrt{\Gamma_1 \Gamma_2}} \sqrt{n_1^0 n_2^0} > 1. \quad (D7)$$

This is essentially the same condition as was found for a single oscillator. We also obtain an expression as a function of the detuning near $\omega_p = 4\Omega$,

$$\Omega_p^2 > \sqrt{\frac{\Gamma_1^2 \omega_p^2}{4} + 16 \left(\Omega^2 - \frac{\omega_p^2}{16} \right)^2}, \quad (D8)$$

where we have assumed for simplicity that $\Gamma_1 = \Gamma_3$.

-
- [1] C. Gerry and P. Knight, *Introductory Quantum Optics* (Cambridge University Press, Cambridge, 2004).
- [2] H. P. Yuen, Two-photon coherent states of the radiation field, *Phys. Rev. A* **13**, 2226 (1976).
- [3] H. P. Yuen and J. H. Shapiro, Generation and detection of two-photon coherent states in degenerate four-wave mixing, *Opt. Lett.* **4**, 334 (1979).
- [4] R. E. Slusher, L. W. Hollberg, B. Yurke, J. C. Mertz, and J. F. Valley, Observation of Squeezed States Generated by Four-Wave Mixing in an Optical Cavity, *Phys. Rev. Lett.* **55**, 2409 (1985).
- [5] L. A. Wu, H. Kimble, J. Hall, and H. Wu, Generation of Squeezed States by Parametric Down Conversion, *Phys. Rev. Lett.* **57**, 2520 (1986).
- [6] S. T. Yang, R. C. Eckardt, and R. L. Byer, Power and spectral characteristics of continuous-wave parametric oscillators: The doubly to singly resonant transition, *J. Opt. Soc. Am. B* **10**, 1684 (1993).
- [7] X. Zeng, and M. A. Popovic, Design of triply-resonant microphotonic parametric oscillators based on Kerr nonlinearity, *Opt. Express* **22**, 15837 (2014).
- [8] H. J. Kimble, The quantum internet, *Nature (London)* **453**, 1023 (2008).
- [9] R. S. Bondurant and J. H. Shapiro, Squeezed states in phase-sensing interferometers, *Phys. Rev. D* **30**, 2548 (1984).
- [10] E. Polzik, J. Carri, and H. J. Kimble, Spectroscopy with Squeezed Light, *Phys. Rev. Lett.* **68**, 3020 (1992).
- [11] B. J. Lawrie, P. D. Lett, A. M. Marino, and R. C. Pooser, Quantum sensing with squeezed light, *ACS Photonics* **6**, 1307 (2019).
- [12] C. S. Hamilton, R. Kruse, L. Sansoni, S. Barkhofen, C. Silberhorn, and I. Jex, Gaussian Boson Sampling, *Phys. Rev. Lett.* **119**, 170501 (2017).
- [13] H.-S. Zhong, H. Wang, Y.-H. Deng, M.-C. Chen, L.-C. Peng, Y.-H. Luo, J. Qin, D. Wu, X. Ding, Y. Hu, P. Hu, X.-Y. Yang, W.-J. Zhang, H. Li, Y. Li, X. Jiang, L. Gan, G. Yang, L. You, Z. Wang *et al.*, Quantum computational advantage using photons, *Science* **370**, 1460 (2020).
- [14] C. C. Ruppel, Acoustic wave filter technology: a review, *IEEE Trans. Ultrason. Ferroelectr. Freq. Control* **64**, 1390 (2017).
- [15] P. Delsing, A. N. Cleland, M. J. A. Schuetz, J. Knärzer, G. Giedke, J. I. Cirac, K. Srinivasan, M. Wu, K. C. Balram, C. Bäuerle, T. Meunier, C. J. B. Ford, P. V. Santos, E. Cerdá-Méndez, H. Wang, H. J. Krenner, E. D. S. Nysten, M. Weiss, G. R. Nash, L. Thevenard *et al.*, The 2019 surface acoustic waves roadmap, *J. Phys. D: Appl. Phys.* **52**, 353001 (2019).
- [16] G. A. Garrett, A. G. Rojo, A. K. Sood, J. F. Whitaker, and R. Merlin, Vacuum squeezing of solids: Macroscopic quantum states driven by light pulses, *Science* **275**, 1638 (1997).

- [17] X. Hu and F. Nori, Phonon squeezed states: quantum noise reduction in solids, *Phys. B: Condens. Matter* **263-264**, 16 (1999).
- [18] M. Aspelmeyer, T. J. Kippenberg, and F. Marquardt, Cavity optomechanics, *Rev. Mod. Phys.* **86**, 1391 (2014).
- [19] T. K. Paraíso, M. Kalaei, L. Zang, H. Pfeifer, F. Marquardt, and O. Painter, Position-Squared Coupling in a Tunable Photonic Crystal Optomechanical Cavity, *Phys. Rev. X* **5**, 041024 (2015).
- [20] J. D. Thompson, B. M. Zwickl, A. M. Jayich, F. Marquardt, S. M. Girvin, and J. G. E. Harris, Strong dispersive coupling of a high-finesse cavity to a micromechanical membrane, *Nature (London)* **452**, 72 (2008).
- [21] T. P. Purdy, D. W. C. Brooks, T. Botter, N. Brahm, Z. Y. Ma, and D. M. Stamper-Kurn, Tunable Cavity Optomechanics with Ultracold Atoms, *Phys. Rev. Lett.* **105**, 133602 (2010).
- [22] N. P. Bullier, A. Pontin, and P. F. Barker, Quadratic optomechanical cooling of a cavity-levitated nanosphere, *Phys. Rev. Research* **3**, L032022 (2021).
- [23] H. Miao, S. Danilishin, T. Corbitt, and Y. Chen, Standard Quantum Limit for Probing Mechanical Energy Quantization, *Phys. Rev. Lett.* **103**, 100402 (2009).
- [24] L. Dellantonio, O. Kyriienko, F. Marquardt, and A. S. Sorensen, Quantum nondemolition measurement of mechanical motion quanta, *Nat. Commun.* **9**, 3621 (2018).
- [25] A. A. Clerk, F. Marquardt, and J. G. E. Harris, Quantum Measurement of Phonon Shot Noise, *Phys. Rev. Lett.* **104**, 213603 (2010).
- [26] M. Bhattacharya, H. Uys, and P. Meystre, Optomechanical trapping and cooling of partially reflective mirrors, *Phys. Rev. A* **77**, 033819 (2008).
- [27] A. Nunnenkamp, K. Borkje, J. G. E. Harris, and S. M. Girvin, Cooling and squeezing via quadratic optomechanical coupling, *Phys. Rev. A* **82**, 021806(R) (2010).
- [28] E. E. Wollman, C. U. Lei, A. J. Weinstein, J. Suh, A. Kronwald, F. Marquardt, A. A. Clerk, and K. C. Schwab, Quantum squeezing of motion in a mechanical resonator, *Science* **349**, 952 (2015).
- [29] X. Ma, J. J. Viennot, S. Kotler, J. D. Teufel, and K. W. Lehnert, Nonclassical energy squeezing of a macroscopic mechanical oscillator, *Nat. Phys.* **17**, 322 (2021).
- [30] I. Carusotto, and C. Ciuti, Quantum fluids of light, *Rev. Mod. Phys.* **85**, 299 (2013).
- [31] J. Kasprzak, M. Richard, S. Kundermann, A. Baas, P. Jembrun, J. M. J. Keeling, F. M. Marchetti, M. H. Szymańska, R. André, J. L. Staehli, V. Savona, P. B. Littlewood, B. Deveaud, and L. S. Dang, Bose-Einstein condensation of exciton polaritons, *Nature (London)* **443**, 409 (2006).
- [32] E. A. Cerda-Méndez, D. N. Krizhanovskii, M. Wouters, R. Bradley, K. Biermann, K. Guda, R. Hey, P. V. Santos, D. Sarkar, and M. S. Skolnick, Polariton Condensation in Dynamic Acoustic Lattices, *Phys. Rev. Lett.* **105**, 116402 (2010).
- [33] G. Rozas, A. E. Bruchhausen, A. Fainstein, B. Jusserand, and A. Lemaître, Polariton path to fully resonant dispersive coupling in optomechanical resonators, *Phys. Rev. B* **90**, 201302(R) (2014).
- [34] B. Jusserand, A. N. Poddubny, A. V. Poshakinskiy, A. Fainstein, and A. Lemaître, Polariton Resonances for Ultrastrong Coupling Cavity Optomechanics in GaAs-AlAs Multiple Quantum Wells, *Phys. Rev. Lett.* **115**, 267402 (2015).
- [35] A. S. Kuznetsov, D. H. O. Machado, K. Biermann, and P. V. Santos, Electrically Driven Microcavity Exciton-Polariton Optomechanics at 20 GHz, *Phys. Rev. X* **11**, 021020 (2021).
- [36] D. L. Chafatinos, A. S. Kuznetsov, S. Anguiano, A. E. Bruchhausen, A. A. Reynoso, K. Biermann, P. V. Santos, and A. Fainstein, Polariton-driven phonon laser, *Nat. Commun.* **11**, 4552 (2020).
- [37] A. S. Kuznetsov, P. L. J. Helgers, K. Biermann, and P. V. Santos, Quantum confinement of exciton-polaritons in structured (Al,Ga)As microcavity, *Phys. Rev. B* **97**, 195309 (2018).
- [38] A. Fainstein, N. D. Lanzillotti-Kimura, B. Jusserand, and B. Perrin, Strong Optical-Mechanical Coupling in a Vertical GaAs/AlAs Microcavity for Subterahertz Phonons and Near-Infrared Light, *Phys. Rev. Lett.* **110**, 037403 (2013).
- [39] S. Anguiano, A. E. Bruchhausen, B. Jusserand, I. Favero, F. R. Lamberti, L. Lanco, I. Sagnes, A. Lemaître, N. D. Lanzillotti-Kimura, P. Senellart, and A. Fainstein, Micropillar Resonators for Optomechanics in the Extremely High 19–95-GHz Frequency Range, *Phys. Rev. Lett.* **118**, 263901 (2017).
- [40] F. Mangussi, D. L. Chafatinos, N. Bolivar, A. A. Reynoso, A. E. Bruchhausen, A. S. Kuznetsov, K. Biermann, P. V. Santos, A. Fainstein, and G. Usaj (unpublished).
- [41] V. Villafañe, P. Sesin, P. Soubelet, S. Anguiano, A. E. Bruchhausen, G. Rozas, C. Gomez Carbonell, A. Lemaître, and A. Fainstein, Optoelectronic forces with quantum wells for cavity optomechanics in GaAs/AlAs semiconductor microcavities, *Phys. Rev. B* **97**, 195306 (2018).
- [42] F. Marquardt, J. G. E. Harris, and S. M. Girvin, Dynamical Multistability Induced by Radiation Pressure in High-Finesse Micromechanical Optical Cavities, *Phys. Rev. Lett.* **96**, 103901 (2006).
- [43] A. Pikovsky, M. Rosenblum, and J. Kurths, *Synchronization: A Universal Concept in Nonlinear Sciences* (Cambridge University Press, Cambridge, 2001).
- [44] M. Wouters, Synchronized and desynchronized phases of coupled nonequilibrium exciton-polariton condensates, *Phys. Rev. B* **77**, 121302(R) (2008).
- [45] H. Ohadi, Y. D. V. I. Redondo, A. J. Ramsay, Z. Hatzopoulos, T. C. H. Liew, P. R. Eastham, P. G. Savvidis, and J. J. Baumberg, Synchronization crossover of polariton condensates in weakly disordered lattices, *Phys. Rev. B* **97**, 195109 (2018).
- [46] I. Kovacic, R. Rand, and S. M. Sah, Mathieu's equation and its generalizations: overview of stability charts and their features, *Appl. Mech. Rev.* **70**, 020802 (2018).
- [47] L. D. Landau and E. M. Lifshitz, *Mechanics* (Pergamon, Oxford, 1960).
- [48] A. Jenkins, Self-oscillation, *Phys. Rep.* **525**, 167 (2013).
- [49] D. Navarro-Urrios, N. E. Capuj, M. F. Colombano, P. D. García, M. Sledzinska, F. Alzina, A. Griol, A. Martínez, and C. M. Sotomayor-Torres, Nonlinear dynamics and chaos in an optomechanical beam, *Nat. Commun.* **8**, 14965 (2017).
- [50] J. Wu, S.-W. Huang, Y. Huang, H. Zhou, J. Yang, J.-M. Liu, M. Yu, G. Lo, D.-L. Kwong, S. Duan, and C. W. Wong, Mesoscopic chaos mediated by Drude electron-hole plasma in silicon optomechanical oscillators, *Nat. Commun.* **8**, 15570 (2017).
- [51] T. F. Roque, F. Marquardt, and O. M. Yevtushenko, Nonlinear dynamics of weakly dissipative optomechanical systems, *New J. Phys.* **22**, 013049 (2020).
- [52] L. Zhang, F. Ji, X. Zhang, and W. Zhang, Photon-phonon parametric oscillation induced by quadratic coupling in an optomechanical resonator, *J. Phys. B: At. Mol. Opt. Phys.* **50**, 145501 (2017).

- [53] A. Smerzi, S. Fantoni, S. Giovanazzi, and S. R. Shenoy, Quantum Coherent Atomic Tunneling between Two Trapped Bose-Einstein Condensates, *Phys. Rev. Lett.* **79**, 4950 (1997).
- [54] M. Albiez, R. Gati, J. Föling, S. Hunsmann, M. Cristiani, and M. K. Oberthaler, Direct Observation of Tunneling and Non-linear Self-Trapping in a Single Bosonic Josephson Junction, *Phys. Rev. Lett.* **95**, 010402 (2005).
- [55] S. Zöllner, H. D. Meyer, and P. Schmelcher, Few-Boson Dynamics in Double Wells: From Single-Atom to Correlated Pair Tunneling, *Phys. Rev. Lett.* **100**, 040401 (2008).
- [56] A. U. Lode, A. I. Streltsov, K. Sakmann, O. E. Alon, and L. S. Cederbaum, How an interacting many-body system tunnels through a potential barrier to open space, *Proc. Natl. Acad. Sci. USA* **109**, 13521 (2012).
- [57] K. G. Lagoudakis, B. Pietka, M. Wouters, R. André, and B. Deveaud-Plödran, Coherent Oscillations in an Exciton-Polariton Josephson Junction, *Phys. Rev. Lett.* **105**, 120403 (2010).
- [58] M. Abbarchi, A. Amo, V. G. Sala, D. D. Solnyshkov, H. Flayac, L. Ferrier, I. Sagnes, E. Galopin, A. Lemaître, G. Malpuech, and J. Bloch, Macroscopic quantum self-trapping and Josephson oscillations of exciton polaritons, *Nat. Phys.* **9**, 275 (2013).
- [59] M. J. Hartmann, F. G. Brandao, and M. B. Plenio, Strongly interacting polaritons in coupled arrays of cavities, *Nat. Phys.* **2**, 849 (2006).
- [60] K. P. Kalinin and N. G. Berloff, Toward arbitrary control of lattice interactions in nonequilibrium condensates, *Adv. Quantum Technol.* **3**, 1900065 (2020).
- [61] S. Alyatkin, H. Sigurdsson, A. Askitopoulos, J. D. Töpfer, and P. G. Lagoudakis, Quantum fluids of light in all-optical scatterer lattices, *Nat. Commun.* **12**, 5571 (2021).
- [62] S. Ghosh and T. C. H. Liew, Quantum computing with exciton-polariton condensates, *npj Quantum Inf* **6**, 16 (2020).
- Correction:* The name of the second author in Ref. 41 was displayed incorrectly due to a production error and has been fixed.